Chemistry–A European Journal
Research Article
doi.org/10.1002/chem.202301241
Chemistry Europe
European Chemical Societies Publishing
www.chemeurj.org

A Novel Nitridoborate Hydride $Sr_{13}[BN_2]_6H_8$ Elucidated from X-ray and Neutron Diffraction Data

Sophia L. Wandelt,[a] Alexander Mutschke,[b, c] Dmitry Khalyavin,[d] Jennifer Steinadler,[a] and Wolfgang Schnick*[a]

Abstract: Metal hydrides are an uprising compound class bringing up various functional materials. Due to the low X-ray scattering power of hydrogen, neutron diffraction is often crucial to fully disclose the structural characteristics thereof. We herein present the second strontium nitridoborate hydride known so far, $Sr_{13}[BN_2]_6H_8$, formed in a solid-state reaction of the binary nitrides and strontium hydride at 950 °C. The crystal structure was elucidated based on single-crystal X-ray and neutron powder diffraction in the hexagonal space group $P6_3/m$ (no. 176), exhibiting a novel three-dimensional network of $[BN_2]^{3-}$ units and hydride anions connected by strontium cations. Further analyses with magic angle spinning (MAS) NMR and vibrational spectroscopy corroborate the presence of anionic hydrogen within the structure. Quantum chemical calculations reveal the electronic properties and support the experimental outcome. $Sr_{13}[BN_2]_6H_8$ expands the emerging family of nitridoborate hydrides, broadening the access to an open field of new, intriguing materials.

Introduction

Convincing with a widespread variety of structural and functional features, the class of metal hydrides is an exciting field of current research. Intriguing properties such as hydrogen storage or luminescence upon doping with Eu^{2+} demonstrate the practical applicability of these materials.[1–2] Moreover, metal hydrides can exhibit fast hydride ion conductivity, enhancing their attractiveness as alternative energy materials for application in solid-state batteries.[3–4] Coming to the characterization of these compounds, the possibilities are limited. Laboratory X-ray diffraction (XRD) studies are often not capable of resolving light elements such as hydrogen or lithium due to their low electron density.[5] In contrast to X-rays, the scattering of neutrons is independent of the atomic number, but varies for each isotope and is influenced, among other factors, by the spin of the nucleus.[6] The coherent scattering length b_c together with the scattering cross section σ describes, how effective the neutrons will be scattered at the respective nucleus, analogous to the atomic form factor for X-ray radiation.[7] However, neutron diffraction allows distinction of neighboring elements such as nitrogen ($b_c = 9.4$ fm) and oxygen ($b_c = 5.8$ fm) and is also sensitive to different isotopes of an element. For instance, ^{10}B has a high σ, a negative b_c and shows strong neutron absorption, whereas ^{11}B has a moderate σ and b_c and is well suited for neutron experiments.[6] Analogously, the two stable isotopes of hydrogen show fundamentally different scattering lengths ($b_c(^1H) = -3.7$ fm, $b_c(^2H) = 6.7$ fm), so that a clear distinction of these nuclei is possible.[6] The peculiarities of certain elements can result in disruptive side effects such as absorption or incoherent scattering, making an isotope modification of the compound often necessary to obtain reliable diffraction data. Once the suitability of the sample is verified, neutron diffraction data can reveal various structural features, such as magnetic properties or superstructures caused by light elements.[8–9] In the case of hydride compounds, neutron data allow for the exact determination of the crystallographic positions, occupancies and atomic parameters of hydrogen or deuterium atoms in the crystal structure. Taking a closer look at their structural motifs, hydridic compounds comprise a large variability of coordination spheres and bonding partners of the hydride anion. Ranging from linear, for example in $LiNiH_3$, over trigonal planar and tetrahedral in $CaAlH_5$ up to octahedral coordination in Ba_2NH, the $M^{\delta+}$–$H^{\delta-}$ distances vary from 1.6 to 3.0 Å, respectively.[10–12] Within this structural diversity, hydrides tend to build compounds with

[a] S. L. Wandelt, J. Steinadler, Prof. Dr. W. Schnick
Department of Chemistry
University of Munich (LMU)
Butenandtstr. 5–13, 81377 Munich, Germany
E-mail: wolfgang.schnick@uni-muenchen.de
[b] Dr. A. Mutschke
Chair of Inorganic Chemistry with Focus in Novel Materials
Department of Chemistry, TU Munich
Lichtenbergstr. 4, 85748 Garching (Germany)
[c] Dr. A. Mutschke
Heinz Maier-Leibnitz Zentrum (MLZ)
TU Munich
Lichtenbergstr. 1, 85748 Garching (Germany)
[d] Dr. D. Khalyavin
Rutherford Appleton Laboratory
ISIS Facility
Didcot OX11 0QX (UK)

Supporting information for this article is available on the WWW under https://doi.org/10.1002/chem.202301241

multiple cations or multiple anions, whereas the latter have gained much interest in research over the last decades. Combining different anions in one material allows tailoring its physical, structural and electronic features.[13] Multinary hydrides are largely dominated by hydride oxides and hydride fluorides due to their similar atomic radii, easy accessibility and high stability.[2,14–15] Other anion combinations such as hydrides and nitridoborates are a less explored class so far. Only two representatives of nitridoborate hydrides have been reported to date, namely Ca_2BN_2H and Sr_2BN_2H, leaving an open field of new functional and structurally diverse materials.[16–17]

Herein, we present the strontium nitridoborate hydride $Sr_{13}[BN_2]_6H_8$, which was synthesized from the respective nitrides and strontium hydride and crystallizes in a new structure type. Single-crystal X-ray and neutron powder diffraction data together with MAS NMR and vibrational spectroscopy provide a comprehensive structural analysis of the compound.

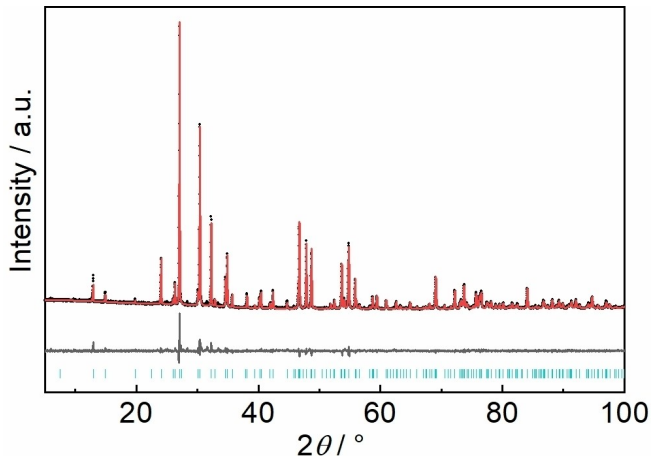

Figure 1. Rietveld refinement of $Sr_{13}[BN_2]_6H_8$ based on powder XRD data. The red, black and gray lines mark the calculated and experimental data and their difference, respectively, the Bragg markers are displayed in blue.

Results and Discussion

Synthesis

Analogous to other nitridoborate hydrides, $Sr_{13}[BN_2]_6H_8$ was synthesized in a solid-state reaction of stoichiometric amounts of Sr_2N, SrH_2 and BN in a sealed tantalum ampule under argon atmosphere at 950 °C. It is highly sensitive to air and moisture and exhibits colorless, block-like crystals up to 50 μm in length. The bulk sample was analyzed by means of powder XRD (Figure 1), showing a high phase purity of $Sr_{13}[BN_2]_6H_8$. The crystallographic data of the Rietveld refinement can be found in Table S1 in the Supporting Information.

Structure elucidation

The crystal structure of the title compound was partially elucidated from single-crystal XRD data (Table 1). Due to the low scattering power of hydrogen, only Sr, B, and N could be refined, building a three-dimensional network in the hexagonal space group $P6_3/m$ (no. 176). To determine the atomic positions of hydrogen in the structure, neutron powder diffraction was performed. As mentioned earlier, ^{1}H has a large incoherent scattering length and ^{10}B acts as a neutron absorber, necessitating a synthesis with ^{11}B and ^{2}H to obtain reliable data. Rietveld refinement of the neutron diffraction pattern (Figure 2, Table 1) led to two crystallographic positions of hydrogen on fully occupied Wyckoff positions 6*h* and 2*d*. Due to minor hydrogen impurities in the starting material ^{11}BN (elemental analysis results are listed in Table S2), the sample could not be completely deuterated, resulting in a sum formula of $Sr_{13}[^{11}BN_2]_6D_{6.8}H_{1.2}$. Both hydrogen positions show a similar mixed occupancy of about 84 % D and 16 % ^{1}H, which implies a formal scattering length of 5.0 fm at each position. As a deuterium deficiency with 75 % vacancies would lead to the exact same scattering length, further analyses were necessary to support the mixed occupation with hydrogen. Infrared spectroscopy (Figure S1) shows that both ^{1}H and D vibrations

Table 1. Crystallographic data of the single-crystal XRD refinement and Rietveld refinement based on neutron powder diffraction data of $Sr_{13}[BN_2]_6H_8$ and $Sr_{13}[^{11}BN_2]_6D_{6.8}H_{1.2}$, respectively. Standard deviations are given in parentheses.

formula	$Sr_{13}[BN_2]_6H_8$	$Sr_{13}[^{11}BN_2]_6D_{6.8}H_{1.2}$
formula mass/g·mol^{-1}	1380.10	1386.95
space group	$P6_3/m$ (no. 176)	
lattice parameters/Å	$a = 13.6724(3)$	$a = 13.6797(1)$
	$b = 3.8831(1)$	$b = 3.8853(4)$
cell volume/Å^3	628.63(3)	629.67(1)
formula units/cell	1	
calculated density/g·cm^{-3}	3.646	3.657
diffractometer	Bruker D8 Venture	ISIS, WISH
radiation	Mo-Kα	neutrons (*tof*)
Temperature/K	297	298
refined parameters	37	47
GooF	1.141	6.129
R indices	$R1$ ($I \geq 2\sigma(I)$) = 0.0177	$R_p = 0.0360$
	$wR2$ ($I \geq 2\sigma(I)$) = 0.0336	$R_{wp} = 0.0398$
	$R1$ (all data) = 0.0233	$R_{exp} = 0.0065$
	$wR2$ (all data) = 0.0345	$R_{Bragg} = 0.0474$

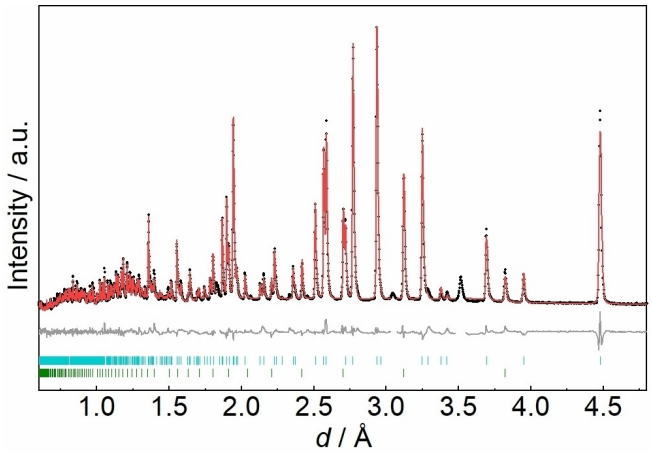

Figure 2. Rietveld refinement of $Sr_{13}[^{11}BN_2]_6D_{6.8}H_{1.2}$ based on time-of-flight neutron powder diffraction data collected at the high-resolution back-scattering detector bank with the average $2\theta = 153°$. The black, red and gray lines mark the experimental and calculated data and their difference, respectively. The Bragg markers indicate $Sr_{13}[^{11}BN_2]_6D_{6.8}H_{1.2}$ (top, 94.7(3) wt-%) and $Sr_3B_2N_4$ (bottom, 5.4(1) wt-%).

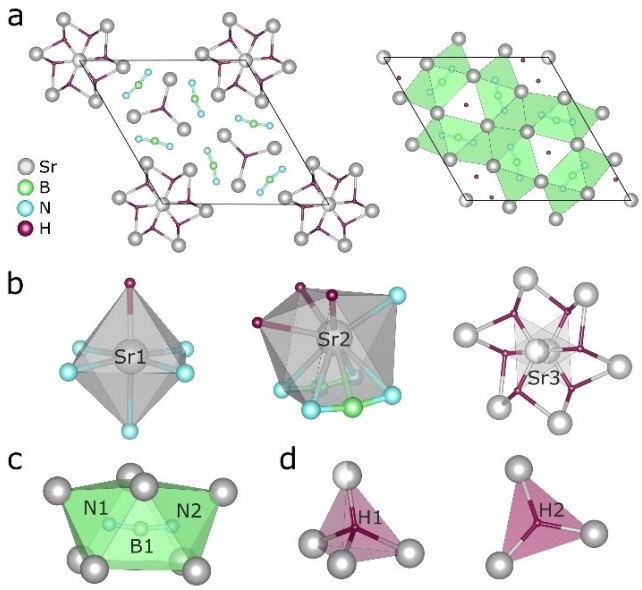

Figure 3. (a) Depiction of the crystal structure of $Sr_{13}[BN_2]_6H_8$ viewing along [001] (b) $Sr(N_5H)$ octahedron, $Sr(N_5B_2H_3)$ polyhedron and Sr_7H_6 star with the strontium split position in the center (c) $[BN_2]^{3-}$ unit coordinated by strontium as a bicapped trigonal prism (d) H^- anions distorted tetrahedrally and trigonally planar coordinated by strontium atoms. The Sr atoms are displayed in gray, B in green, N in blue and H in purple.

are shifted by a factor of $\sqrt{2}$ due to the difference in atomic mass, indicating the presence of ^1H in the sample. Additionally, the ^1H MAS NMR data show the same two signals as the non-deuterated compound (Figure S2 and Figure 5). Taking these analyses and charge balance into account, a deuterium deficiency cannot be fully excluded but seems unlikely. Similarly, the related compound Sr_2BN_2H already showed the same issue upon deuteration, resulting in a partially mixed occupation of ^1H and D.[16] The atomic positions, occupations and displacement parameters of XRD and neutron data refinements of $Sr_{13}[BN_2]_6H_8$ and $Sr_{13}[^{11}BN_2]_6D_{6.8}H_{1.2}$, respectively, are listed in Tables S3 and S4 in the Supporting Information.

Structure description

$Sr_{13}[BN_2]_6H_8$ reveals a three-dimensional network of hydride and nitridoborate anions, connected by strontium cations (Figure 3a). Along the *c* axis, all atoms build one-dimensional stacks. The $[BN_2]^{3-}$ units are coordinated by eight strontium cations which build a channel-like network incorporating the hydride ions. Sr1 is coordinated as a slightly distorted $Sr(N_5H)$ octahedron, while Sr2 shows a 10-fold coordination by two full $[BN_2]^{3-}$ units, one N^{3-} of another $[BN_2]^{3-}$ unit and three H^- ions (Figure 3b). The Sr–N bond lengths are in the range of 2.541(3)–3.061(3) Å, agreeing with literature data.[18–20] In the middle of the Sr_7H_6 stars in the corners of the unit cell appears a strontium split position (Sr3) with 50% occupancy, trigonally planar coordinated by hydride ions. The slightly bent $[BN_2]^{3-}$ units are coordinated in a bicapped trigonal prism (Figure 3c), as already observed in β-$Ba_3[BN_2]_2$.[21] The N–B–N angle is 166.8(4)° and the B–N bond lengths range from 1.329(6) to 1.339(5) Å, in good agreement with other nitridoborates.[17,19] The hydride anions are trigonally planar and distorted tetrahedrally (Figure 3d) coordinated by strontium, showing bond lengths of 2.13(5)–2.60(5) Å, in accord with literature values.[16,22]

The formation of a previously unknown structure type, differentiates $Sr_{13}[BN_2]_6H_8$ from other nitridoborates such as the closely related nitridoborate hydrides Ca_2BN_2H and Sr_2BN_2H.[16–17] Most alkali and alkaline earth nitridoborates crystallize in the cubic structure types of $Sr_3[BN_2]_2$ and $LiCa_4[BN_2]_3$, showing a high symmetry and linear $[BN_2]^{3-}$ units.[23–24] In contrast, nitridoborate halides often exhibit slightly bent $[BN_2]^{3-}$ units and lower symmetry, building a more versatile group of akin structures.[19,25–26] As hydrides are closely related to halides – especially fluorides – the class of nitridoborate hydrides follows this trend. By combining known building blocks into a novel network type, $Sr_{13}[BN_2]_6H_8$ extends the family of structural intriguing nitridoborate compounds.

Vibrational spectroscopy

IR and Raman spectroscopy are other suited methods to support the structure model due to the vibrational activity of both hydride and nitridoborate anions.[17,27–28] The experimental FTIR spectrum of $Sr_{13}[BN_2]_6H_8$ (Figure 4) agrees well with the simulated one obtained by DFT calculations at the PBE0 level of theory, showing the characteristic vibrations of the $[BN_2]^{3-}$ units and H^- atoms. The N–B–N vibrations are visible at 1668 cm^{-1} (antisymmetrical stretching, ν_2) and 600 cm^{-1} (in- and out-of-plane bending, ν_3), according to other known nitridoborates.[16–17] The hydride in-plane and out-of-plane vibrations arise at 1002, 889, 851 and 767 cm^{-1}, also in good

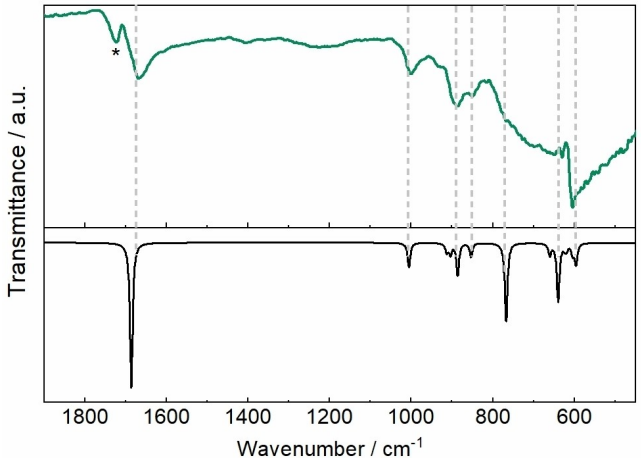

Figure 4. Experimental (top) and simulated (bottom) FTIR spectrum of $Sr_{13}[BN_2]_6H_8$. The band marked with an asterisk arises from the IR active side phase $Sr_3B_2N_4$.

agreement with literature.[16] Minor contaminations of $Sr_3B_2N_4$ cause the weak band at 1724 cm^{-1}. Furthermore, the presence of a NH^- or OH^- species can be ruled out, as there are no vibrational bands detectable in the region of 3600–3200 cm^{-1} (Figure S3). The Raman spectrum of the title compound (Figure S4 in the Supporting Information) shows the symmetrical N–B–N stretching and H^- in-plane vibration at 1061 cm^{-1} as well as the N–B–N in-plane bending and H^- in-plane vibration at 615 and 591 cm^{-1}. The expected hydride in-plane and out-of-plane vibrations in the region of 800–900 cm^{-1} remain rather broad and unresolved in contrast to the simulated spectrum. Below 300 cm^{-1}, the N–B–N in-plane and out-of-plane vibrations as well as the isotropic lattice vibrations are observable. The plane of the vibrations is described by the Sr atoms and the assignment of all vibrations is listed in Tables S5 and S6.

MAS NMR

^1H and ^{11}B MAS NMR measurements were performed to support the proposed structure model. The ^1H spectrum (Figure 5, top) shows two signals at 6.4 and 5.4 ppm, which is consistent with the presence of two crystallographically independent hydrogen positions in the structure. The signals are shifted towards the lower magnetic field, an effect already observed for other salt-like hydride species.[27,29–30] The MAS spectrum of ^{11}B ($I = 3/2$) shows the central-transition resonance, which exhibits second order broadening due to the quadrupolar interaction (Figure 5, bottom). The position of this resonance line is determined by the quadrupolar interaction and the chemical shift, so a fit of the spectrum is required to extract the numerical values of these NMR parameters. This was done using the DMFIT program, and the resulting values are listed in Table 2.[31] For comparison, we have fitted the previously published ^{11}B NMR spectrum of Sr_2BN_2H, which also contains slightly bent $[BN_2]^{3-}$ ions.[16] The ^{11}B MAS NMR spectrum of the related compound

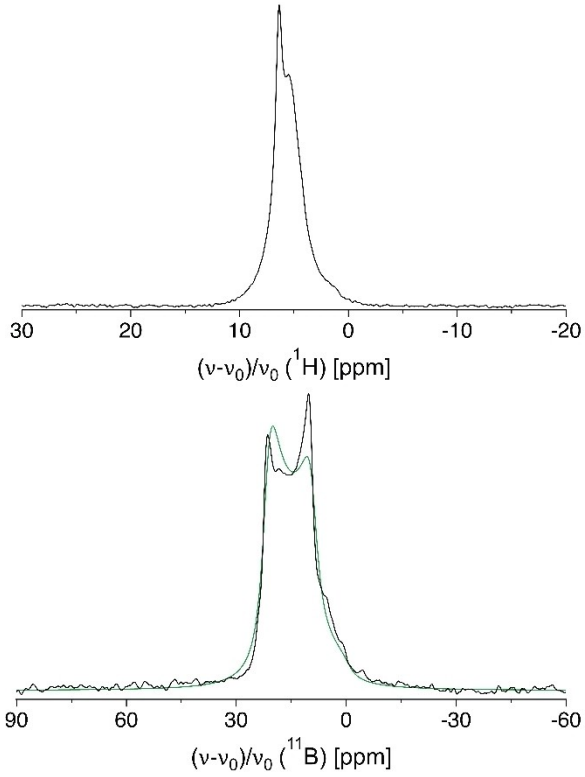

Figure 5. MAS NMR spectra of $Sr_{13}[BN_2]_6H_8$ at 20 kHz spinning frequency. ^1H (top) and ^{11}B spectrum (bottom), the latter shown with the best fitting result (green line).

Table 2. Calculated values of the chemical shift, quadrupole coupling constant and asymmetry parameter for $SrBa_8[BN_2]_6$, Sr_2BN_2H and $Sr_{13}[BN_2]_6H_8$. *NMR parameters reported here for the first time.

compound	δ_{iso}/ppm	C_Q/MHz	η_Q	∢(N–B-N)/°	Ref.
$SrBa_8[BN_2]_6$	26.6	3.30	0.02	180	[32]
Sr_2BN_2H	23.6	3.31	0.04	174.9	[16]*
$Sr_{13}[BN_2]_6H_8$	25.2	3.25	0.09	166.8	this work*

$SrBa_8[BN_2]_6$ published by Seidel et al. provides another comparison.[32] As expected for the nearly linear structural motif of N–B–N, the quadrupole coupling constant is rather large, with values beyond 3 MHz, rarely observed in periodic solids.[33] In contrast, the asymmetry parameter is close to zero, reflecting the axial symmetry of the $[BN_2]^{3-}$ ions, which are indeed perfectly linear in $SrBa_8[BN_2]_6$. The slight bend of the N–B–N units in the other compounds could tentatively correlate to an increase in the asymmetry parameter (Table 2). However, it should be noted that the quality of the ^{11}B spectra recorded for all listed compounds is not sufficient to determine the asymmetry parameter with high accuracy.

Electronic properties

Quantum chemical calculations at DFT-PBE0 level of theory were performed to analyze the electronic and vibrational

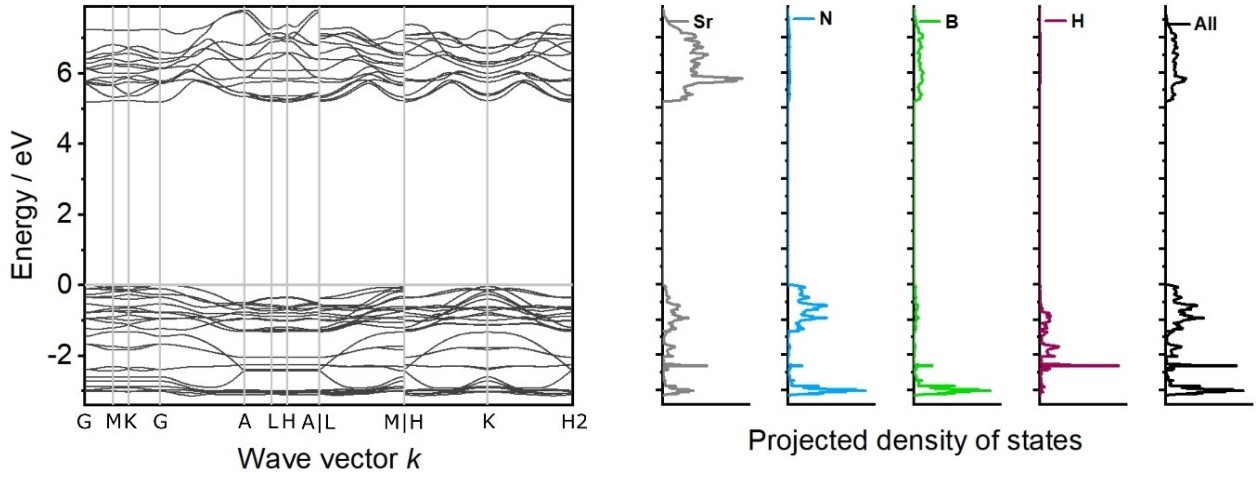

Figure 6. Electronic band structure and projected density of states of $Sr_{13}[BN_2]_6H_8$ calculated at the DFT-PBE0/TZVP level of theory.

properties of $Sr_{13}[BN_2]_6H_8$. However, due to the disorder of the Sr3 position, an ordered model of the experimentally determined crystal structure was employed. By lowering the symmetry to the space group *P*3 (no. 143), the disorder was removed and an averaged Sr3 position (Sr5 in the new model) was established. The ordered model was optimized and appears to be a local minimum with no imaginary frequencies. Compared to the experimental data, the optimized lattice parameters *a* and *c* of the ordered model deviate by −0.05% and −0.2%, respectively. The calculated electronic band structure (Figure 6, left) indicates a direct bandgap of 5.2 eV. This is reflected by the colorless and transparent appearance of $Sr_{13}[BN_2]_6H_8$, classifying this compound as an insulator. Similar to Sr_2BN_2H, mostly nitrogen states contribute to the top of the valence band in the projected density of states (Figure 6, right) with only minor contributions from the other elements.[16] However, the hydrogen bands emerge predominantly at lower energies, contrary to other known multinary hydride compounds.[34–35]

Conclusion

In this contribution, we present the novel strontium nitridoborate hydride $Sr_{13}[BN_2]_6H_8$ accessed in a solid-state reaction of the respective binary nitrides and strontium hydride. The crystal structure was solved using a combination of single-crystal X-ray and neutron powder diffraction data, revealing a novel three-dimensional network of nitridoborate and hydride anions connected by strontium cations. The powerful and necessary method of neutron diffraction confirms the atomic positions of hydrogen and corroborates the crystal structure in the hexagonal space group $P6_3/m$ (no. 176). Together with other analyses such as MAS NMR and vibrational spectroscopy, we provide a complete structural and analytical proof of hydride anions in the compound. Quantum chemical DFT calculations support the experimental results and reveal the electronic structure of $Sr_{13}[BN_2]_6H_8$. Such hydrogen-rich compounds bear a promising potential to be utilized as hydride ion conducting materials, as it has been demonstrated for several other hydridic compounds.[36–37] Considering the substantial structural and functional diversity mentioned above, the family of multinary hydrides offers great potential for new intriguing applications.

Experimental Section

Synthesis: The preparation and analyses of all samples were performed in Argon-filled gloveboxes (Unilab, MBraun, Garching, $H_2O < 1$ ppm, $O_2 < 1$ ppm) due to the moisture and air sensitivity of the starting materials and products. Strontium subnitride was prepared in a radio frequency furnace (IG 10/600; Hüttinger Elektronik, Freiburg, Germany) from granulated strontium metal (Sigma-Aldrich, 99.99%) in nitrogen atmosphere at 1000 °C for 24 h, analogous to DiSalvo et al. but at an elevated temperature.[20] Strontium hydride and deuteride were synthesized from strontium metal (Sigma-Aldrich, 99.99%) in an autoclave reaction in hydrogen (Westfalen AG, 99.9%) or deuterium (Airliquide, 99.8%) atmosphere at 60 bar and 450 °C for 15 h.[35] Boron nitride and ^{11}boron nitride were obtained in an ammonia gas flow reaction of boric acid (Sigma-Aldrich, ≥99%) or ^{11}boric acid (Sigma-Aldrich, ≥99%) at 800 °C with 1 equiv. of urea (Sigma-Aldrich, >99.5%) acting as a catalyst.[38] The title compound $Sr_{13}[BN_2]_6H_8$ and its analogous deuteride $Sr_{13}[^{11}BN_2]_6D_{6.8}H_{1.2}$ were synthesized in a solid-state reaction from Sr_2N, SrH_2 (SrD_2) and BN (^{11}BN) with a stoichiometry of 5:3:5. After grinding, the powder was transferred in a tantalum ampoule, which was then weld shut in an arc furnace (Handy-TIG 210 DC, LORCH, Auenwald-Mittelbrüden, Germany). The ampoule was subsequently placed in a silica tube and heated at 950 °C for 20 h in a tube furnace (Carbolite Gero, Neuhausen, Germany). The purity of all materials was analyzed by powder X-ray diffraction.

Single-Crystal XRD: A single crystal of $Sr_{13}[BN_2]_6H_8$ was isolated under argon atmosphere, transferred to a glass capillary and then sealed airtight. Diffraction data were collected on a Bruker D8 VENTURE diffractometer using a rotating anode and Mo-Kα radiation. The program package APEX3 was used for integration

and absorption correction.[39–41] The structure solution and refinement was performed with SHELXS and SHELXL using direct methods and the least-squares method.[42–43]

Deposition Number(s) 2239357 ($Sr_{13}[BN_2]_6H_8$) and 2239358 ($Sr_{13}[^{11}BN_2]_6D_{6.8}H_{1.2}$) contain(s) the supplementary crystallographic data for this paper. These data are provided free of charge by the joint Cambridge Crystallographic Data Centre and Fachinformationszentrum Karlsruhe Access Structures service.

Powder XRD: To analyze the bulk composition of each sample, the powder was ground and sealed in a glass capillary. The data were collected using a STOE Stadi P diffractometer with Cu-Kα_1 radiation, a Ge(111) monochromator, and a Mythen1K detector in modified Debye–Scherrer geometry. TOPAS6 was used for Rietveld refinements with a fundamental parameters approach and a shifted Chebyshev function for the background.[44–45]

Neutron Powder Diffraction: The deuterated compound $Sr_{13}[^{11}BN_2]_6D_{6.8}H_{1.2}$ was loaded in a 6 mm vanadium can and then sealed with an indium wire. Time-of-flight neutron data were obtained using the WISH diffractometer at ISIS pulsed neutron source (STFC, Rutherford Appleton Laboratory, Harwell Campus, UK).[46] The program package FullProf was used for Rietveld refinement with a fundamental parameters approach and convolution of pseudo-Voigt with back-to-back exponential functions for profile fitting.[45,47] A coherent scattering length $b_c = 6.65(4)$ fm was used for refining ^{11}B.[6]

Fourier-Transform Infrared Spectroscopy: Infrared spectra of the samples were collected on a Bruker Alpha II FTIR spectrometer using a diamond attenuated total reflectance (ATR) unit. All spectra were recorded in a glovebox in the range of 450–4000 cm^{-1} and with a resolution of 2 cm^{-1}.

Raman Spectroscopy: The Raman spectrum of a powder sample of $Sr_{13}[BN_2]_6H_8$ was measured with a Renishaw inVia Reflex Raman System in sealed glass capillaries in the range of 100–1200 cm^{-1} using a laser with a wavelength of $\lambda = 532$ nm and a charge-coupled device detector.

Magic Angle Spinning Nuclear Magnetic Resonance (MAS NMR): Solid-state MAS NMR data were obtained using a 2.5 mm ZrO_2 rotor in a Bruker 500 AVANCE-III spectrometer operating at 500 MHz. The spectra were recorded at a spinning frequency of 20 kHz using a 2.5 μs 90° pulse, and were referenced indirectly to ^1H in 100% TMS.

Quantum Chemical Calculations: The geometry, electronic and vibrational properties of the title compound were studied by density functional theory calculations conducted with the CRYSTAL17 program package at the DFT-PBE0 level of theory.[48–50] A full description of the computational analysis can be found in the Supporting Information.

Supporting Information

Additional references cited within the Supporting Information.[35,48–58]

Acknowledgements

The authors gratefully acknowledge the ISIS Neutron and Muon Source for granting beamtime (Proposal no. 2220086) and Christian Minke (Department of Chemistry, LMU Munich) for the MAS NMR measurements. Open Access funding enabled and organized by Projekt DEAL.

Conflict of Interests

The authors declare no conflict of interest.

Data Availability Statement

The data that support the findings of this study are available in the supplementary material of this article.

Keywords: hydrides · nitridoborates · neutron diffraction · MAS NMR · DFT

[1] B. Chao, L. Klebanoff, *Hydrogen Storage in Interstitial Metal Hydrides*, CRC Press, Florida **2012**.
[2] N. Kunkel, H. Kohlmann, *J. Phys. Chem. C* **2016**, *120*, 10506–10511.
[3] A. J. E. Rowberg, C. G. V. d Walle, *ACS Appl. Energ. Mater.* **2021**, *4*, 6348–6355.
[4] Y. Yu, W. Zhang, H. Cao, T. He, P. Chen, *Trends Chem.* **2022**, *4*, 935–947.
[5] W. I. F. David, K. Shankland, L. B. McCusker, C. Baerlocher, *Structure Determination from Powder Diffraction Data*, University Press, Oxford **2002**.
[6] V. F. Sears, *Neutron News* **1992**, *3*, 26–37.
[7] L. Koester, *Neutron Scattering Lengths and Fundamental Neutron Interactions*, Springer Verlag, Berlin **1977**.
[8] K. Higashi, M. Ochi, Y. Nambu, T. Yamamoto, T. Murakami, N. Yamashina, C. Tassel, Y. Matsumoto, H. Takatsu, C. M. Brown, H. Kageyama, *Inorg. Chem.* **2021**, *60*, 11957–11963.
[9] A. V. Irodova, E. Suard, *J. Alloys Compd.* **1999**, *291*, 184–189.
[10] R. Sato, H. Saitoh, N. Endo, S. Takagi, M. Matsuo, K. Aoki, S.-I. Orimo, *Appl. Phys. Lett.* **2013**, *102*, 091901.
[11] C. Weidenthaler, T. J. Frankcombe, M. Felderhoff, *Inorg. Chem.* **2006**, *45*, 3849–3851.
[12] F. Altorfer, W. Bührer, B. Winkler, G. Coddens, R. Essmann, H. Jacobs, *Solid State Ionics* **1994**, *70*, 272–277.
[13] H. Kageyama, K. Hayashi, K. Maeda, J. P. Attfield, Z. Hiroi, J. M. Rondinelli, K. R. Poeppelmeier, *Nat. Commun.* **2018**, *9*, 772.
[14] C. E. Messer, *J. Solid State Chem.* **1970**, *2*, 144–155.
[15] Y. Iwasaki, N. Matsui, K. Suzuki, Y. Hinuma, M. Yonemura, G. Kobayashi, M. Hirayama, I. Tanaka, R. Kanno, *J. Mater. Chem. A* **2018**, *6*, 23457–23463.
[16] S. L. Wandelt, A. Karnas, A. Mutschke, N. Kunkel, C. Ritter, W. Schnick, *Inorg. Chem.* **2022**, *61*, 12685–12691.
[17] M. Somer, Ö. Yaren, O. Reckeweg, Y. Prots, W. Carrillo-Cabrera, *Z. Anorg. Allg. Chem.* **2004**, *630*, 1068–1073.
[18] S. G. Jantz, R. Erdmann, S. Hariyani, J. Brgoch, H. A. Höppe, *Chem. Mater.* **2020**, *32*, 8587–8594.
[19] F. Rohrer, R. Nesper, *J. Solid State Chem.* **1998**, *135*, 194–200.
[20] O. Reckeweg, F. J. DiSalvo, *Solid State Sci.* **2002**, *4*, 575–584.
[21] O. Reckeweg, F. J. DiSalvo, M. Somer, *J. Alloys Compd.* **2003**, *361*, 102–107.
[22] B. Blaschkowski, T. Schleid, *Z. Anorg. Allg. Chem.* **2007**, *633*, 2644–2648.
[23] H. Womelsdorf, H.-J. Meyer, *Z. Anorg. Allg. Chem.* **1994**, *620*, 262–265.
[24] M. Somer, U. Herterich, J. Curda, W. Carrillo-Cabrera, A. Zürn, K. Peters, H. G. v Schnering, *Z. Anorg. Allg. Chem.* **2000**, *626*, 625–633.
[25] M. Somer, M. N. Kütükcü, R. C. Gil, H. Borrmann, W. Carrillo-Cabrera, *Z. Anorg. Allg. Chem.* **2004**, *630*, 1015–1021.
[26] I. Kokal, U. Aydemir, Y. Prots, W. Schnelle, L. Akselrud, P. Höhn, M. Somer, *Z. Kristallogr.* **2011**, *226*, 633–639.
[27] A. Mutschke, G. M. Bernard, M. Bertmer, A. J. Karttunen, C. Ritter, V. K. Michaelis, N. Kunkel, *Angew. Chem.* **2021**, *60*, 5683–5687.
[28] A. Mutschke, A. Schulz, M. Bertmer, C. Ritter, A. J. Karttunen, G. Kieslich, N. Kunkel, *Chem. Sci.* **2022**, *13*, 7773–7779.
[29] Y. Ruiz-Morales, G. Schreckenbach, T. Ziegler, *Organometallics* **1996**, *15*, 3920–3923.

[30] K. Hayashi, P. V. Sushko, Y. Hashimoto, A. L. Shluger, H. Hosono, *Nat. Commun.* **2014**, *5*, 3515.
[31] D. Massiot, F. Fayon, M. Capron, I. King, S. L. Calvé, B. Alonso, J. O. Durand, B. Bujoli, Z. Gan, G. Hoatson, *Magn. Reson. Chem.* **2002**, *40*, 70–76.
[32] S. Seidel, T. Dierkes, T. Jüstel, C. Benndorf, H. Eckert, R. Pöttgen, *Dalton Trans.* **2016**, *45*, 12078–12086.
[33] Y.-T. A. Wong, D. L. Bryce, *Annu. Rep. NMR Spectrosc.* **2018**, *93*, 213–279.
[34] T. Wu, A. Ishikawa, T. Honda, H. Tamatsukuri, K. Ikeda, T. Otomo, S. Matsuishi, *RSC Adv.* **2020**, *9*, 5282–5287.
[35] T. Wylezich, R. Valois, M. Suta, A. Mutschke, C. Ritter, A. Meijerink, A. J. Karttunen, N. Kunkel, *Chem. Eur. J.* **2020**, *26*, 11742–11750.
[36] Q. Bai, X. He, Y. Zhu, Y. Mo, *ACS Appl. Energ. Mater.* **2018**, *1*, 1626–1634.
[37] T. Hirose, T. Mishina, N. Matsui, K. Suzuki, T. Saito, T. Kamiyama, M. Hirayama, R. Kanno, *ACS Appl. Energ. Mater.* **2022**, *5*, 2968–2974.
[38] A. F. Holleman, N. Wiberg, *Lehrbuch der Anorganischen Chemie*, Walter de Gruyter, Berlin, Germany **2007**.
[39] Bruker-AXS, APEX3, Vers. 2016.5-0, Karlsruhe, Germany **2016**.
[40] Bruker-AXS, XPREP Reciprocal Space Exploration, Vers. 6.12, Karlsruhe, Germany **2001**.
[41] G. M. Sheldrick, SADABS Version 2: Multi-Scan Absorption Correction, Bruker-AXS, Madison, Wisconsin, USA **2012**.
[42] G. M. Sheldrick, SHELXS - A Program for Crystal Structure Solution, University of Göttingen, Göttingen, Germany **1997**.
[43] G. M. Sheldrick, *Acta Crystallogr. Sect. A* **2008**, *64*, 112–122.
[44] A. Coelho, TOPAS-Academic V6.1, Coelho Software, Brisbane, Australia **2007**.
[45] H. M. Rietveld, *J. Appl. Crystallogr.* **1969**, *2*, 65–71.
[46] L. C. Chapon, P. Manuel, P. G. Radaelli, C. Benson, L. Perrott, S. Ansell, N. J. Rhodes, D. Raspino, D. Duxbury, E. Spill, J. Norris, *Neutron News* **2011**, *22*, 22–25.
[47] J. Rodriguez-Carvajal, *Physica B + C* **1993**, *192*, 55–69.
[48] R. Dovesi, A. Erba, R. Orlando, C. M. Zicovich-Wilson, B. Civalleri, L. Maschio, M. Rérat, S. Casassa, J. Baima, S. Salustro, B. Kirtman, *Wiley Interdiscip. Rev.: Comput. Mol. Sci.* **2018**, *8*, e1360.
[49] J. P. Perdew, K. Burke, M. Ernzerhof, *Phys. Rev. Lett.* **1996**, *77*, 3865–3868.
[50] C. Adamo, V. Barone, *J. Chem. Phys.* **1999**, *110*, 6158–6170.
[51] F. Weigend, R. Ahlrichs, *Phys. Chem. Chem. Phys.* **2005**, *7*, 3297–3305.
[52] A. J. Karttunen, T. Tynell, M. Karppinen, *J. Phys. Chem. C* **2015**, *119*, 13105–13114.
[53] H. J. Monkhorst, J. D. Pack, *Phys. Rev. B* **1976**, *13*, 5188–5192.
[54] A. Togo, I. Tanaka, **2018**, arXiv preprint arXiv:1808.01590.
[55] Y. Hinuma, G. Pizzi, Y. Kumagai, F. Oba, I. Tanaka, *Comput. Mater. Sci.* **2017**, *128*, 140–184.
[56] F. Pascale, C. M. Zicovich-Wilson, F. L. Gejo, B. Civalleri, R. Orlando, R. Dovesi, *J. Comput. Chem.* **2004**, *25*, 888–897.
[57] C. M. Zicovich-Wilson, F. Pascale, C. Roetti, V. R. Saunders, R. Orlando, R. Dovesi, *J. Comput. Chem.* **2004**, *25*, 1873–1881.
[58] L. Maschio, B. Kirtman, M. Rérat, R. Orlando, R. Dovesi, *J. Chem. Phys.* **2013**, *139*, 164101.

Manuscript received: April 19, 2023
Accepted manuscript online: May 24, 2023
Version of record online: June 13, 2023